Supplementary Information

Highly Sensitive and Wide-Band Tunable Terahertz Response of Plasma Wave based on Graphene Field Effect Transistors

Lin Wang, Xiaoshuang Chen*, Anqi Yu, Yang Zhang, Jiayi Ding and Wei Lu

National Laboratory for Infrared Physics, Shanghai Institute of Technical Physics, Chinese Academy of Sciences, 500 Yu Tian Road, Shanghai, Shanghai 200083, China
Synergetic Innovation Center of Quantum Information & Quantum Physics, University of Science and Technology of China, Hefei, Anhui 230026, China

S1. 2D plasma waves in graphene FETs

Plasma waves in 2D electron gas system have been intensively studied more than 30 years since the discovery of its excitation in Si inversion layer[1]. It results from the periodic motion of electrons in response to the local ac field (F_{restore}), during the process, the electrons are pulled back and front by the disturbed local charges, setting up the weakly damped oscillation. In the long-wavelength limit (plasma wavevector $q<<k_F$, k_F is Fermi wavevector), the macroscopic description of plasma waves based on hydrodynamic is good agreement with the dielectric theory or RPA (random phase approximation)[2, 3]. The deviation of electron density from average value $\delta n(\boldsymbol{r}, t)$ and the associated current density δj ($\boldsymbol{r}$, t) under the plasmonic action are described by the linearized Euler equation of motion and continuity equation (seeing Materials and Methods). With this condition, the dispersion relationship of plasma waves in 2D electron gas is given in the first order approximation $\omega_{\text{pl}}=(e^2 n_s q/2m_b\varepsilon^*)^{0.5}$, where m_b and ε^* are the effective mass and permittivity of Schödinger fermions, respectively, n_s is sheet density of the 2D electron gas. Thus, the frequency of plasma wave can be tuned in proportional to the square root of n_s with parabolic dispersion. The situation turns out to be quite different for massless Dirac fermions in graphene. An immediate consequence is that the cyclotron mass depends on square root of the electronic density. Thus, the Drude-weight of plasma waves is given by $e^2E_F/\pi\hbar^2$, which is also proportional to $n_s^{0.5}$. In the long-wavelength limit, the frequency in doped graphene is $\omega_{\text{pl}}=(e^2E_Fq/2\ \pi\hbar^2\varepsilon^*)^{0.5}$, similar to that of previous report on the plasmon at the interface between two dielectric medium[4]. Therefore, the phase velocity of plasma waves is determined mainly by two important parameters, the effective permittivity ε^* and Fermi energy E_F.

In the typical structure with continuous monolayer graphene either (chemical vapor deposition) CVD grown or mechanically exfoliated on substrate such as SiO_2 or hexagonal-boron-nitride (hBN), the velocity of plasma waves can exceeds 5×10^8cm/s with the Fermi energy 0.1eV. The result indicates that the response time can be less than 1ps in large-scale graphene device arrays with the unit element exceeds 5μm. To realize the THz detectors based on the principle of hydrodynamic nonlinearity (seeing Materials and Methods), a device array with aperture comparable with incoming waves would be preferred. Thus, in comparison with other already available ones, the graphene-based plasma wave device contains technological advantages of

robust and can be flexibly engineered with Si CMOS process.

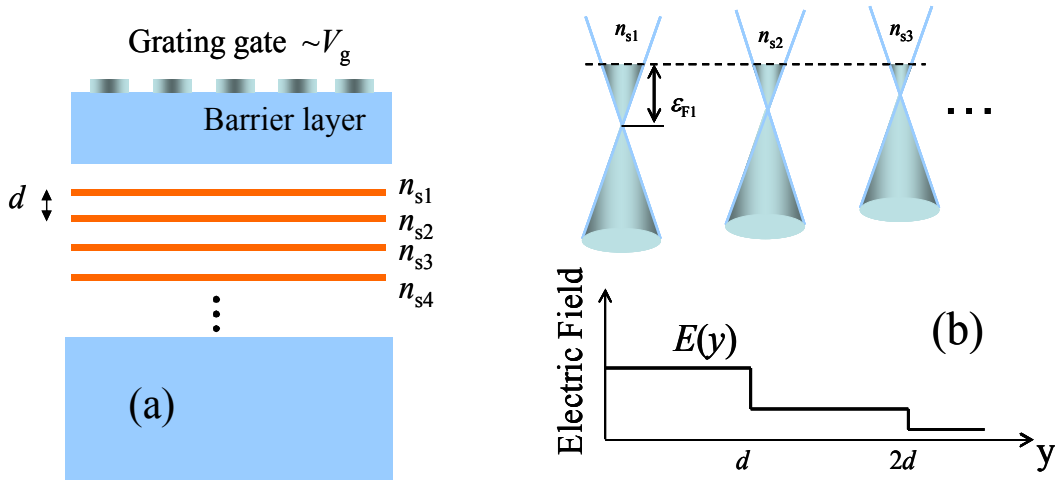

Fig. S1. (a) Schematic of MGL field effect transistor with dielectric barrier layer d separating the electrodes from the graphene-channels. (b) The distribution of Fermi energy and electric field between the two neighboring graphene layers under the electrostatic doping.

S2. Electrostatic screening of Graphene layers

Recent success in fabricating high-quality multiple graphene layers (MGLs) stimulates great interests in perspective of multiple-GL devices[5, 7]. In addition, the multilayer graphene systems have been proposed for inhibiting the effects of the substrate and noise[7]. The complication in studying graphene multilayers is the coupling interaction between the neighbor graphene layers. For Bernal stacking (A-B), half the carbon atoms in each hexagon of the top layer are located exactly over the center of the hexagon layer below. The stack results in strong coupling between the two layers and tunable bandgap under strong electric field. We consider the rhombohedral stacking multilayers obtained by thermal decomposition or furnace-grown[8] on carbon terminated SiC. Following the well-established experimental fact, the structures constitute the stacks of disoriented GLs, and each GL exhibits linear dispersion relation for electrons and holes with extreme long electron momentum relaxation time, in similar to that in single GL. Electrostatic screening in multilayer graphene is highly nonlinear due to the linear dispersion of electronic spectrum. Here we calculate the interlayer screening in MGL field effect transistor, as shown in Fig. S1, with the potential distribution in the y direction governed by the Poisson equation,

$$\frac{d^2\psi}{dz^2} = \frac{e}{\varepsilon_0 \varepsilon} \sum_{k=1}^{K} (n - p) \cdot \delta(y - kd) \tag{1}$$

where, ε_0 and ε is the vacuum permittivity and dielectric constant, n and p are the equilibrium sheet densities of electrons and holes in the kth GL, respectively. These densities after taking into account the dispersion spectrum of MGL device, are expressed with Fermi energy as,

$$n, p = \frac{2}{(2\pi\hbar)^2}\int d^2\mathbf{p} f_{e,h}$$
$$f_{e,h} = \left[1+\exp\left(\frac{v_F p \mp \varepsilon_F}{k_B T}\right)\right]^{-1} \quad (2)$$

The boundary conditions are assumed to be as follows,

$$\Psi(y)|_{y=0} = V_g + W_g(d\Psi/dy)_{y=0}\ ;\ (d\Psi/dy)_{y=Kd}=0; \quad (3)$$

By solving the Eqs. (1) to (3), the screening among MGLs under different gate voltages can be obtained. As shown in Fig. S2, the screening is highly nonlinear due to the linear energy dispersion of electron. It is noted that the screening effect depends strongly on the number of graphene layers and the Fermi energy is declined rapidly in the device with increasing graphene layers. The result indicates that the effective screening length $\lambda_{eff}^{i,i+1} = d/\log(q_i/q_{i+1})$ between i and i+1 layer is reduced in MGLs in consistent with the experimental results[9]. The phenomenon can be understood intuitively by considering the total screened charge $Q_0 = CV_g$ on the electrodes. By increasing the number of graphene layers, the average electric field among first several graphene layers should become stronger. The result leads to the upshift of the Hartree band and the decrease of density of state. Therefore, the screening length should be reduced through increasing the number of graphene layers. In Fig. S2, we show the results obtained from the continuum model in which the graphene layers are treated as the usual bulk semiconductor,

$$\frac{d^2\psi}{dz^2} = \frac{\psi^2}{L_s^2},\quad L_S = \hbar v_F\sqrt{\frac{\varepsilon_0\varepsilon d}{2e^3 V_g}} \quad (4)$$

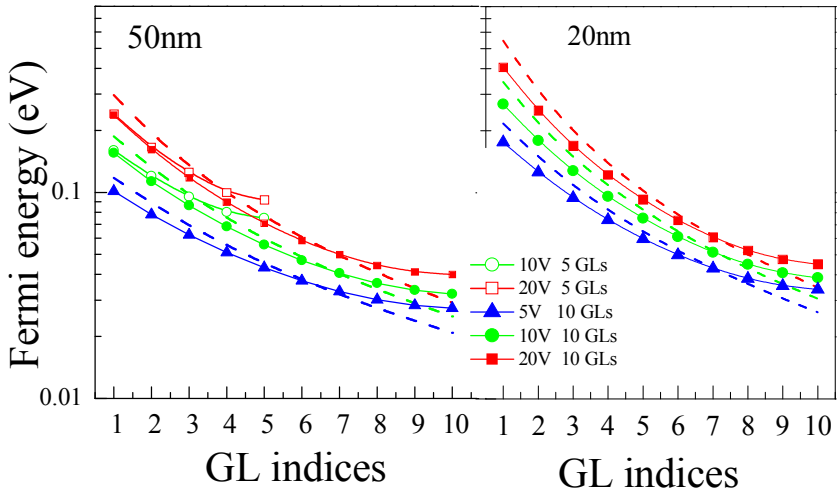

Fig. S2. The screening between graphene layers in MGL device under different gate voltages (solid symbols), left and right columns are MGLs with 50nm and 20nm dielectric barrier layer separating the channels from electrodes, respectively. Both the figures show the similar behavior, and the dashed lines are obtained from continuum dielectric model (Eq. 4).

We can see that the results of such continuum model can qualitatively agree well with that discussed above since the interlayer spacing between two graphene layers is around 3Å.

Fig. S3. (c) shows the distribution of Fermi energy relative to the charge neutral point under different gate voltage with 50nm thick tunneling barrier consisting of h-BN. As can be seen, the

Fermi energy can still be tuned in a relative wide range in double-layer structure. However, in the triple-layer structure, the second and third graphene layers cannot be tuned efficiently even with only an additional atom layer. The result is caused by the screening as discussed above. It should be noted that the tunability is an important issue in the optoelectronic applications of graphene device. Thus, we propose to control the multi-graphene layers separately by the electrodes and make use of the unique advantages of mechanical flexibility of graphene for multi-layer device. Such a device can be fabricated by transferring the h-BN layer, with controllable thickness down to several atomic layers, onto the graphene sheets prepared with using either mechanical cleavage or epitaxial grown.

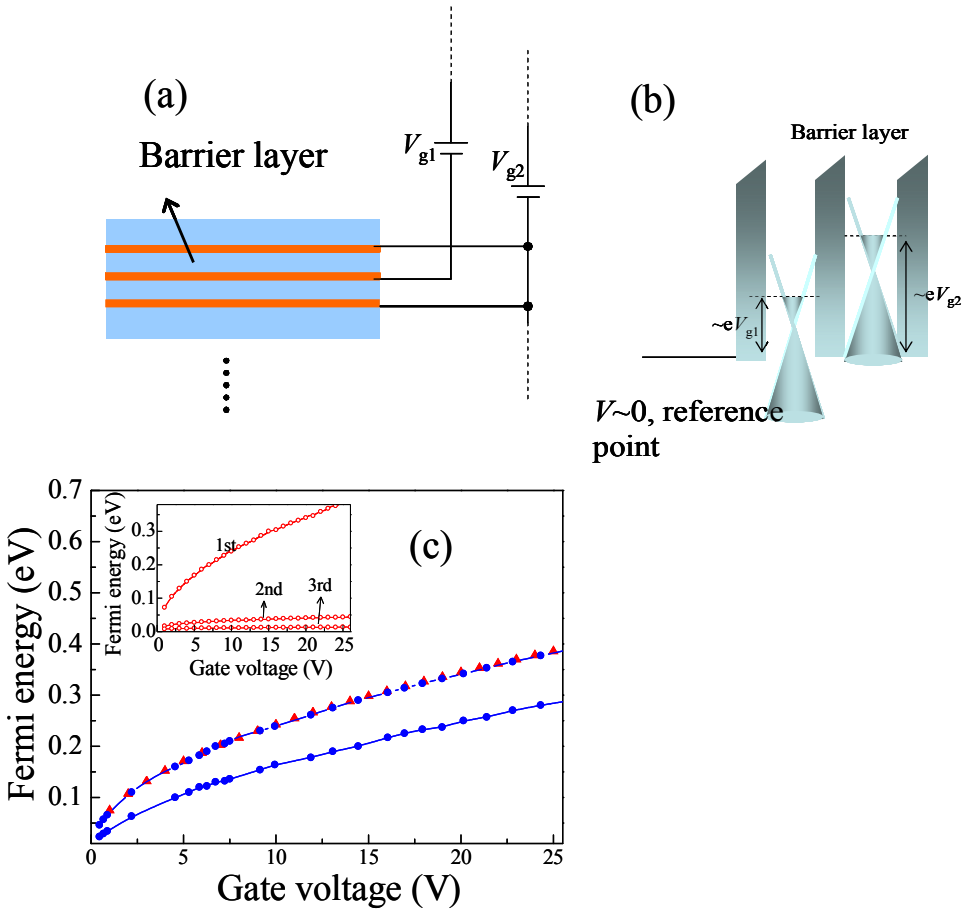

Fig. S3. (a) MGL device with tunneling barrier structure, all the graphene layers are controlled separately by the gate voltage. (b) Schematic of the Fermi energy distribution and the energy band structure in reference to the zero potential point. (c) The distribution of Fermi energy in double and triple layer (inset) graphene device with tunneling barrier structure under different gate voltages, as shown in Fig. S1 (a).

S3. Tunable THz waveguide based on the FET

The effective medium theorem in the Materials and Methods can be represented by the strong dependence of plasma wave propagation on structural parameters, or in other words, the screening of surrounding media. Fig.S4 displays the propagation of plasma waves with wavevector[10] $q\sim(1-1/\alpha^2)^{-0.5}$ ($\alpha=2\pi\sigma/c$, σ is the graphene conductivity) along two kind configurations of waveguide structure, one is the multiple-waveguide like structure as shown in Fig. 3g, and the other one is the structure with square-wave grating substrate. It should be noted that stronger confinement of graphene plasma wave can be realized by reducing the channel length L to around ~400nm. From the color-plot of Fig. 3(h) of the text, the resonant intensity varies non-monotonously when the thickness d_{ox} of gate oxide increases. The maxima of plasma wave resonance corresponds to the balance between strong plasma wave confinement in a less lossy sheet (50nm <d_{ox}<200nm) and smaller confinement in a more absorbing sheet (smaller d_{ox}<50nm) in similar to the results shown in Ref. 10. Correspondingly, the propagation of plasma waves is affected by the absorption and depends nonmonotonously on the oxide thickness. Figs. S4(a) to (c) show the intensity of electric field along the channel in correspondence to d_{ox} of 50nm, 80nm and 800nm, respectively. The minimum propagation distance among Figs.S4 (a), (b) and (c) is in accordance with the strongest absorption region in Fig. 3(h), and it is further confirmed by the decay rate of normalized electric field shown in Fig. S4(f). Similar phenomenon is also observed in the device with square-wave grating substrate, while the leakage of plasma wave into unfilled region/grooves forms another energy-loss channel in addition to the dissipation of electron scattering. Generally, the absorption and resonant position of plasma wave in this configuration depends on the depth of grooves and period of square-wave grating below the graphene sheet. According to the effective medium theorem, stronger confinement of plasma wave can be done by increasing the depth h of grooves. Although we do not show here, the simulation results of such configuration are in well consistent with Ref. 11, that is, an increased depth h leads to stronger absorption. In Fig.S4g, one can see the decrease of propagation length when the depth increases from 100nm to 800nm.

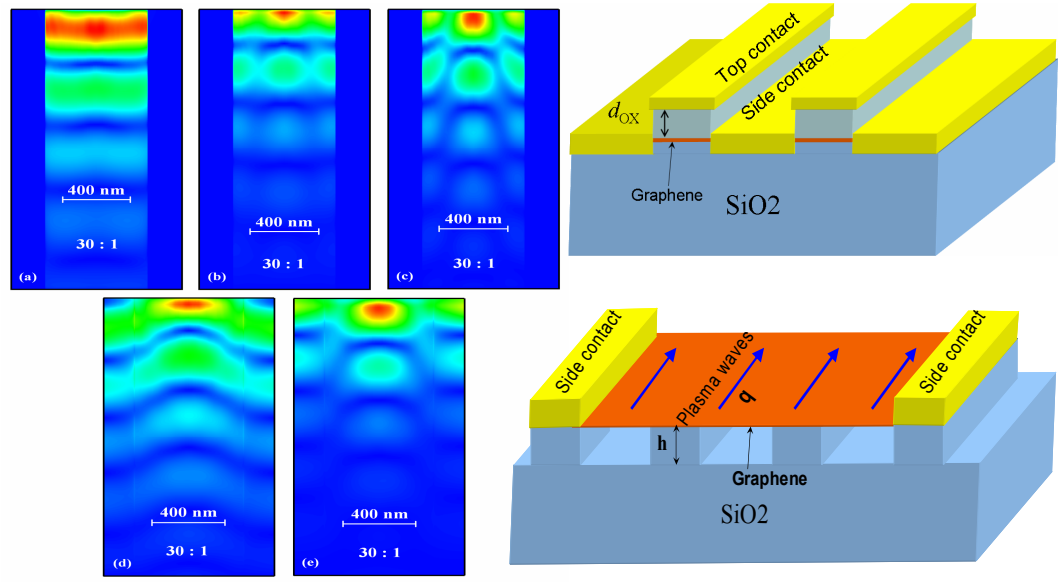

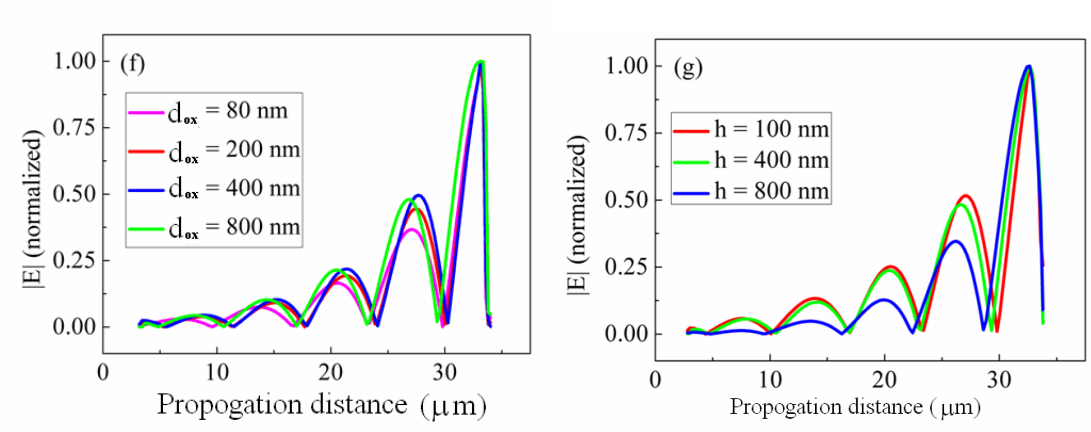

Fig. S4. (a), (b) and (c) are the distributions of the electric field along the multiple-waveguide like FET (Fig. 3(g)), with gate oxide thickness (a) 50nm, (b) 80nm and (c) 800nm, respectively. (d) and (e) are the colorplot of electric field distributions along the square-wave grating structure, with the depth of grooves at 100nm (d) and 800nm (e), respectively. (f) and (g) are the normalized field decay rate with the propagation distance at different gate oxide thickness d_{ox} and depth *h* of grooves, respectively.

References:

1. Allen, S. J., Jr, Tsui, D. C., Logan, R. A. Observation of the two-dimensional plasmon in Silicon inversion layers. *Phys. Rev. Lett.* **38**, 980-982 (1977).

2. Wang, L. et al. Plasmon resonant excitation in grating-gated AlN barrier transistors. *Appl. Phys. Lett.* **100**, 123501-1-123501-5 (2012).

3. Stern, F. Polarizability of a two-dimensional electron gas. *Phys. Rev. Lett.* **18**, 546-548 (1967).

4. Jablan, M., Buljan, H., Soljačić, M. Plasmonics in graphene at infrared frequencies. *Phys. Rev. B.* **80**, 245435-1-7 (2009).

5. Orlita, M., Potemski, M. Dirac electronic states in graphene systems: optical spectroscopy studies. *Semicond. Sci. Technol.* **25**, 063001 (2010).

6. Berger, C. et al. Electronic confinement and coherence in patterned epitaxial graphene. *Science*. **312**, 1191-1195 (2006).

7. Liu, G., Rumyantsev, S., Shur, M., Balandin, A. A. Graphene thickness-graded transistors with reduced electronic noise. *Appl. Phys. Lett.* **100**, 033103 (2012).

8. Hass, J. et al. Why multilayer graphene on 4*H*-SiC(0001) behaves like a single sheet of graphene. *Phys. Rev. Lett.* **100**, 125504 (2008).

9. Kuroda, Marcelo A., Tersoff, J., Martyna, Glenn J. Nonlinear screening in multilayer graphene system. *Phys. Rev. Lett.* **106**, 116804 (2011).

10. Nikitin, A. Yu., Guinea, F., García-Vidal, Martín-Moreno, L. Edge and waveguide terahertz surface plasmon modes in graphene micro-ribbons. *Phys. Rev. B (R)*. **84**, 161407 (2011).

11. Peres, N. M. R., Bludov, Yu V.,Ferreira, A., Vasilevskiy, M. I. Exact solution for square-wave grating covered with graphene: surface Plasmon-polaritons in the terahertz range, *J. Phy.: Condens. Matter*, **25**, 125303 (2013).